spectral characteristics (blue points). Right: Result of region growing and merging of the central building (blue points).

The minimum bounding box of the building region is defined, and pixels on the border, i.e. probably mixed pixels are assigned to the sides of the rectangle. Assigning pixels according to the diagonal of the minimum bounding box or according to the minimal distance, did not show any significant difference in the results. The building boundaries are computed using weighted LS adjustment. In Figure 4 (left) the outbound of the building and both inner yards are independently calculated. The rotation of the northern inner yard compared to the building's main orientation is clearly seen. In Figure 4 (right), we set that the outside boundaries must be parallel to the inner yards, and therefore no rotation is present.

Figure 4: Result of building boundary approximation with sub-pixel accuracy (yellow lines). Outer and inner building boundaries are: independently adjusted (left), and adjusted with the condition that they have the same orientation (right).

On the second example, an outbound of the U-shape building is approximated. The seed points are selected from WV2 DSM, because they could not be chosen from CartoSat DSM due to the high noise. The adjusted boundaries of the building outbound are marked yellow in Figure 5.

Figure 5: Building boundary approximation (left, yellow lines), and comparison of size with laser DSM (right).

3.3 Discussion

The building regions are needed to localize and describe the shapes of the buildings. The regions are defined by the seeded region growing and are dependant on the quality of the initial seed selection. Thus, the outliers among seeds are removed using statistical testing. The Thompson Tau statistics penalize more points as outliers as minimum needed and is therefore an appropriate test statistics. Furthermore, the seeds are selected as local highest points in the DSMs. Both used DSMs were automatically computed and include inaccuracies and noise (Figure 6) which are influencing the selection of local high points. The buildings in CartoSat DSM (blue) have rounded borders, often reaching beyond the real boundaries. This can be observed in Figure 6 by comparing the widths of the building on the left or in the middle to the other DSMs (grey, green). In addition, some errors appear, e.g. a part of the building in the middle of Figure 2 (left) is missing. The seed selection from CartoSat DSM is possible only for the larger and wider buildings, due to the 5 m resolution. The WV2 DSM has a spatial resolution of about 1 m, so seeds on smaller buildings are found. However, the consequence of high frequency noise present in the WV2 DSM (Figure 6, grey) is that some local high points are not on the building roofs, but on the streets (Figure 2, right). The applied region growing is highly dependant on the used DSM. To define building regions more robust, other classification techniques should be considered. However, the main focus of this research is the boundary estimation in HSI images using spectral information, and not the classification of HSI images.

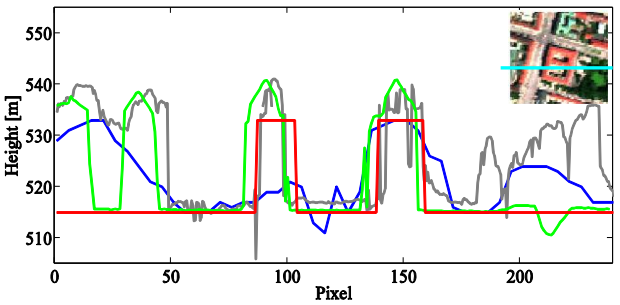

Figure 6: Comparison of approximated building boundaries and DSMs in vertical profile (the position of the profile is marked on the upper right image with a cyan line). CartoSat DSM (blue), WV2 DSM (gray), laser DSM (green) and approximated building boundaries (red) of the building in the centre.

The comparison between vertical profiles of all used DSMs and the adjusted building boundaries is shown in Figure 6. The seed points are selected from CartoSat DSM (blue), and the height of the adjusted building (red) is set to the highest point of this building in the CartoSat DSM. The shift between the profiles is due to the accuracy of georeferencing. The width of the estimated building boundaries in the profile is similar compared to the reference laser DSM (green). The numerical comparison of sizes, i.e. width and length of estimated buildings with the sizes in reference is given in Table 1. For both examples, the outbound of the buildings are estimated better than a pixel. The difference in the roof area between reference and approximated building boundaries is 4% (Figure 4) and 1% (Figure 5, left).

	Laser DSM	**Approximated**	
		no condition	with condition
	Building (Figure 4) length [m] x width [m]		
Outbound	85.6 x 69.2	85 x 69	85 x 69
Yard north	36.3 x 17.2	35 x 14	35 x 14
Yard south	43.2 x 29.4	42 x 28	43 x 28
	Building (Figure 5) length [m] x width [m]		
Outbound	87.2 x 55.5	89 x 55	-

Table 1: The sizes of the approximated buildings from HSI image with spatial resolution of 4 m, compared to the sizes of buildings in laser DSM.

The used LS adjustment is accurate, if redundancy of the measurements is high and observations are free of outliers. The sensitivity of LS adjustment to the low number of redundant measurements is seen on Figure 4 (left) where the north inner yard is rotated and shrinked (Table 1). Only three pixels were assigned to the west border of the north inner yard. In addition, when closely observing the spectral signatures of the mixed pixels on the border of this inner yard, their shape is

significantly more similar to the roof pixels and not to the pavement material. We assume this is a consequence of the sensor or not removed atmospheric influences. The similar effect is present on the borders of the first building southeast of the approximated building (Figure 5). The used spectral similarity SAM for weights has a benefit of being nearly illumination independent, but does not provide the real material abundances.

4. CONCLUSIONS AND FUTURE WORK

We developed an automatic method for sub-pixel building edge detection in HSI images using spectral and spatial information. The roofing materials in HSI images are defined solely with support of height data and without training samples or existing spectral libraries. The building edges are approximated with sub-pixel accuracy using weighted LS method. The weights are derived for each building separately, using spectral information of the mixed pixels on the building borders.

The first results of the proposed building boundary estimation method are promising. The relative accuracy of estimated building outbound for the shown examples is ¼ of a pixel, which corresponds to 1 m for the used HSI data. A further investigation and comparison of building boundary approximation should be made, defining weights with spectral unmixing, other similarity measures or soft classification techniques. Furthermore, the method should be tested on larger urban areas and extended to approximate more complex buildings, e.g. rectilinear or polygonal.

We expect to receive this year the HSI data from Hyspex sensor with 0.5 m spatial resolution. Thus, the potential of the proposed method is to estimate the building boundaries with accuracy comparable to laser DSM. Furthermore, the building roofs can be modelled automatically using combination of the HSI and DSM data.

ACKNOWLEDGEMENTS

The author would like to thank and acknowledge the support of her mentor Prof. Dr. R. Bamler and supervisor Mr. R. Müller. She is a member of the TUM Graduate School and the DLR Graduate Program.

REFERENCES

Baldridge, A.M. et al., 2009. The ASTER spectral library version 2.0. *Remote Sensing of Environment*, 113(4), pp. 711-715.

Braun, A.C., Weidner, U., Jutzi, B., Hinz, S., 2011. Integrating model knowledge into SVM classification - Fusing hyperspectral and laserscanning data by kernel composition. In: ISPRS Hannover Workshop 2011.

Camps-Valls, G., Bruzzone, L., 2005. Kernel-based methods for hyperspectral image classification. *IEEE Transactions on Geoscience and Remote Sensing*, 43(6), pp. 1351- 1362.

Canny, J., 1986. A Computational Approach to Edge Detection. *IEEE Transactions on Pattern Analysis and Machine Intelligence*, 8(6), pp. 679-698.

Chang, Chein-I., 2000. An information-theoretic approach to spectral variability, similarity, and discrimination for hyperspectral image analysis. *IEEE Transactions on Information Theory*, 46(5), pp. 1927-1932.

Chen, P.F., Tran, T.C., 1994. Hyperspectral imagery classification using a backpropagation neural network. In: *IEEE International Conference on Neural Networks*, Vol. 5, pp. 2942-2947.

Evans, A.N., Liu, X.U., 2006. A morphological gradient approach to color edge detection. *IEEE Transactions on Image Processing*, 15(6), pp. 1454-1463.

Gruen, A., Kuebler, O., Agouris, P., 1995. Automatic Extraction of Man-Made Objects from Aerial Space Images. Birkhäuser Verlag, Basel, Boston, Berlin.

Huertas, A., Nevatia, R., Landgrebe, D., 1999. Use of hyperspectral data with intensity images for automatic building modeling. In: *Proc. of the Second International Conference on Information Fusion*, pp. 680–687.

Keshava, N., 2003. A survey of spectral unmixing algorithms. *Lincoln Laboratory Journal*, 14(1), pp. 55–78.

Kruse, F.A. Lefkoff A.B., Boardman J.W., et al., 1993. The spectral image processing system (SIPS) - interactive visualization and analysis of imaging spectrometer data. *Remote Sensing of Environment*, 44(2-3), pp. 145-163.

Mayer, M., 1999. Automatic Object Extraction from Aerial Imagery - A Survey Focusing on Buildings. *Computer Vision and Image Understanding*, 74(2), pp. 138-149.

Mikhail E., Ackerman E.F., 1976. Observations and least squares. IEP, New York, pp. 213-255.

Shaw, G., Manolakis, D., 2002. Signal processing for hyperspectral image exploitation. IEEE *Signal Processing Magazine*, 19(1), pp.12-16.

Sohn, G., Dowman, I., 2007. Data fusion of high-resolution satellite imagery and LiDAR data for automatic building extraction. *ISPRS Journal of Photogrammetry and Remote Sensing*, 62(1), pp. 43-63.

Tarabalka, Y., Benediktsson, J.A., Chanussot, J., Tilton, J.C., 2010. Multiple Spectral–Spatial Classification Approach for Hyperspectral Data. *IEEE Transactions on Geoscience and Remote Sensing*, 48(11), pp. 4122-4132.

Tarabalka, Y., Chanussot, J., Benediktsson, J.A., Angulo, J., Fauvel, M., 2008. Segmentation and Classification of Hyperspectral Data using Watershed. In: *IEEE International Geoscience and Remote Sensing Symposium*, Vol. 3., pp. 652-655.

Villa, A., Chanussot, J., Benediktsson, J.A., Jutten, C., 2011. Spectral Unmixing for the Classification of Hyperspectral Images at a Finer Spatial Resolution. *IEEE Journal of Selected Topics in Signal Processing*, 5(3), pp. 521-533.

Vincent, L., 1993. Morphological grayscale reconstruction in image analysis: applications and efficient algorithms. *IEEE Transactions on Image Processing*, 2(2), pp. 176-201.